



# QSIprep: an integrative platform for preprocessing and reconstructing diffusion MRI data

Matthew Cieslak<sup>1</sup>✉, Philip A. Cook<sup>1</sup>, Xiaosong He<sup>1</sup>, Fang-Cheng Yeh<sup>2</sup>, Thijs Dhollander<sup>3</sup>, Azeez Adebimpe<sup>1</sup>, Geoffrey K. Aguirre<sup>1</sup>, Danielle S. Bassett<sup>1</sup>, Richard F. Betzel<sup>4</sup>, Josiane Bourque<sup>1</sup>, Laura M. Cabral<sup>2</sup>, Christos Davatzikos<sup>1</sup>, John A. Detre<sup>1</sup>, Eric Earl<sup>5</sup>, Mark A. Elliott<sup>1</sup>, Shreyas Fadnavis<sup>4</sup>, Damien A. Fair<sup>6</sup>, Will Foran<sup>2</sup>, Panagiotis Fotiadis<sup>1</sup>, Eleftherios Garyfallidis<sup>4</sup>, Barry Giesbrecht<sup>7</sup>, Ruben C. Gur<sup>1</sup>, Raquel E. Gur<sup>1</sup>, Max B. Kelz<sup>1</sup>, Anisha Keshavan<sup>8</sup>, Bart S. Larsen<sup>1</sup>, Beatriz Luna<sup>2</sup>, Allyson P. Mackey<sup>1</sup>, Michael P. Milham<sup>9</sup>, Desmond J. Oathes<sup>1</sup>, Anders Perrone<sup>5,6</sup>, Adam R. Pines<sup>1</sup>, David R. Roalf<sup>1</sup>, Adam Richie-Halford<sup>8</sup>, Ariel Rokem<sup>8</sup>, Valerie J. Sydnor<sup>1</sup>, Tinashe M. Tapera<sup>1</sup>, Ursula A. Tooley<sup>1</sup>, Jean M. Vettel<sup>10</sup>, Jason D. Yeatman<sup>11</sup>, Scott T. Grafton<sup>7</sup> and Theodore D. Satterthwaite<sup>1</sup>✉

**Diffusion-weighted magnetic resonance imaging (dMRI) is the primary method for noninvasively studying the organization of white matter in the human brain. Here we introduce QSIprep, an integrative software platform for the processing of diffusion images that is compatible with nearly all dMRI sampling schemes. Drawing on a diverse set of software suites to capitalize on their complementary strengths, QSIprep facilitates the implementation of best practices for processing of diffusion images.**

The principal tool for noninvasive studies of white matter organization in humans is dMRI. In recent years, dMRI methods have proliferated as the technology has advanced<sup>1–4</sup> (Supplementary Note 1). However, rapid progress has also yielded disparate acquisition schemes, analysis approaches and file formats that are frequently incompatible. As a result, most research teams tend to use a limited set of methods, without capitalizing on the complementary capabilities of different tools.

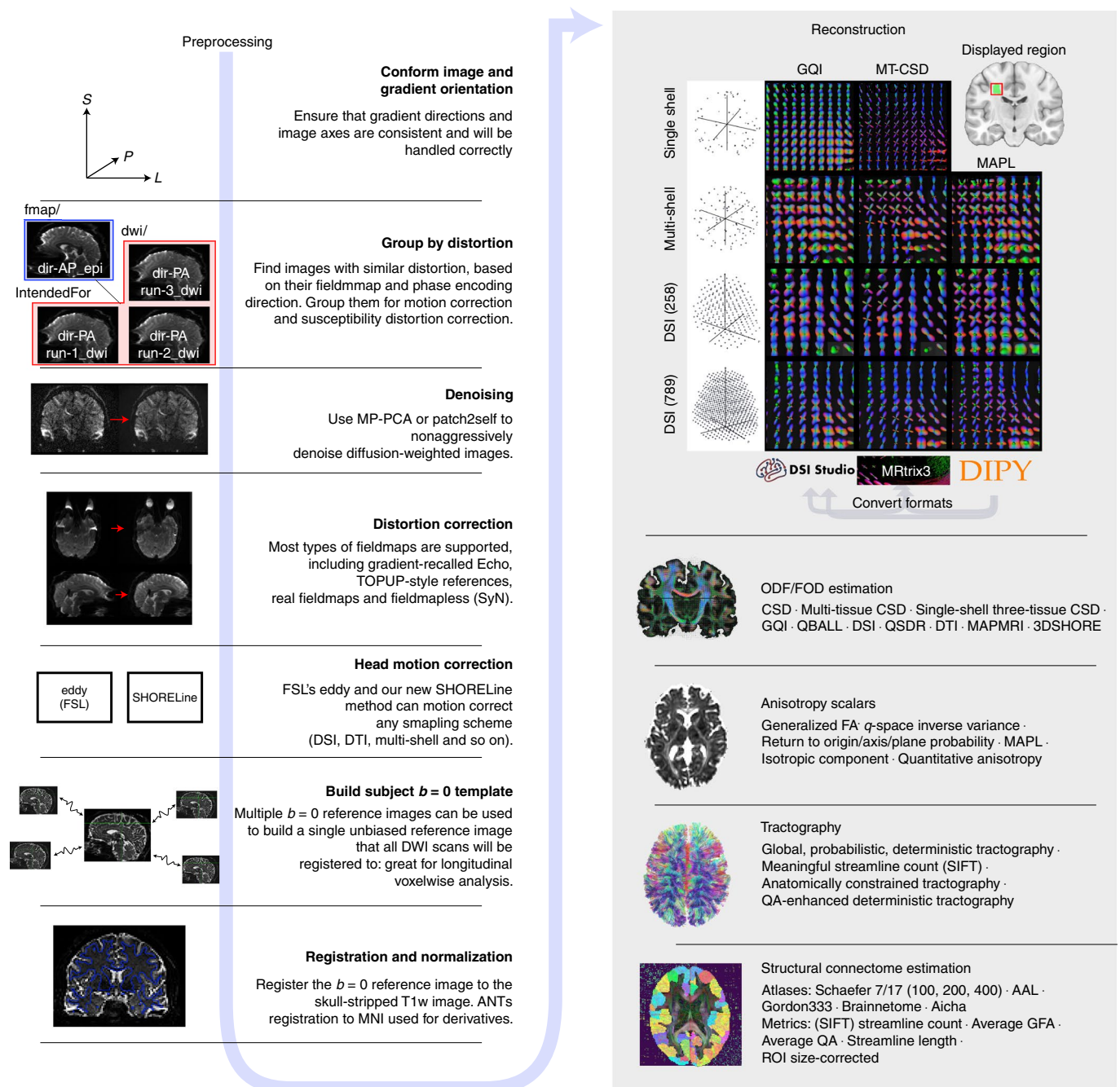
In response to these obstacles, we introduce QSIprep, a unified and robust platform for processing and reconstructing nearly all dMRI data (Fig. 1). QSIprep leverages the metadata recorded in the brain imaging data structure (BIDS)<sup>5</sup> to automatically configure appropriate preprocessing workflows based on the data provided. Furthermore, QSIprep includes curated reconstruction workflows (Supplementary Table 1) that consume the output from QSIprep's preprocessing pipeline and implement advanced reconstruction and tractography methods. Both preprocessing pipelines and reconstruction workflows are fully documented by animated 'before versus after' visual reports at each step, as well as standardized text that details the methods used (Supplementary Figs. 1 and 2 and Supplementary Note 2). Throughout, QSIprep converts data to a consistent, interoperable format to capitalize on the diverse strengths of top software packages (for example, FSL<sup>6</sup>, DSI Studio<sup>7</sup>, DIPY<sup>8</sup>, ANTs<sup>9</sup> and MRtrix<sup>10</sup>).

QSIprep is distributed as both a Python package and as a Docker container that includes the necessary dependencies, ensuring that it is able to run on most computing systems<sup>11</sup>. QSIprep has been publicly available since December 2019. Continuous integration testing, modular design and an open development environment have enabled rapid bug detection and integration of feature requests from its user base.

To illustrate the generalizability of QSIprep to various static *q*-space sampling schemes, we processed eight different datasets acquired with a wide range of acquisition parameters and scanning platforms (*n*=655 total scans). The acquisition schemes for these datasets included a standard single-shell sequence<sup>12</sup>, four different multi-shell sampling schemes<sup>13–16</sup>, two Cartesian grid diffusion spectrum images (DSI) with different sampling densities, as well as a compressed-sensing DSI (CS-DSI) sequence with random *q*-space sampling<sup>17</sup> (Extended Data Fig. 1). We compared the performance of QSIprep to published pipelines tailored for each dataset on two outcomes: image smoothness and image quality.

We characterized the spatial smoothness of the image series by the mean of the estimated full-width at half-maximum (FWHM) smoothness of the *b*=0 images. This measure is affected by multiple interpolations and imprecise spatial resampling of images, which introduce artifactual blurriness that reduces image contrast and anatomic detail. We evaluated the neighboring diffusion-weighted imaging correlation (NDC) as the image quality metric<sup>18</sup>. NDC summarizes the pairwise spatial correlation between each pair of dMRI volumes that sample the closest points in *q*-space; lower values reflect reduced data quality, driven by noise and misalignment between dMRI volumes. While denoising<sup>19,20</sup> and motion correction will increase NDC, it can also be artificially inflated by interpolation-driven spatial smoothing. Accordingly, we regressed image smoothness from the NDC values before comparing pipelines (Supplementary Note 3).

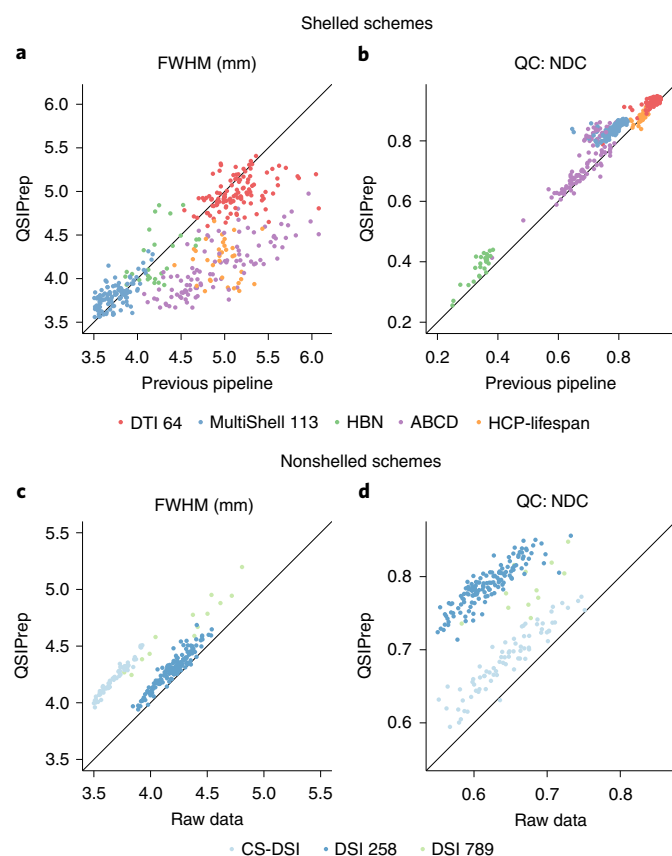
<sup>1</sup>University of Pennsylvania, Philadelphia, PA, USA. <sup>2</sup>University of Pittsburgh, Pittsburgh, PA, USA. <sup>3</sup>Murdoch Children's Research Institute, Melbourne, Victoria, Australia. <sup>4</sup>Indiana University, Bloomington, IN, USA. <sup>5</sup>Oregon Health and Science University, Portland, OR, USA. <sup>6</sup>University of Minnesota, Minneapolis, MN, USA. <sup>7</sup>University of California, Santa Barbara, Santa Barbara, CA, USA. <sup>8</sup>University of Washington, Seattle, WA, USA. <sup>9</sup>Child Mind Institute, New York, NY, USA. <sup>10</sup>Army Research Laboratory, Aberdeen, MD, USA. <sup>11</sup>Stanford University, Stanford, CA, USA. ✉e-mail: [matthew.cieslak@pennmedicine.upenn.edu](mailto:matthew.cieslak@pennmedicine.upenn.edu); [sattertt@pennmedicine.upenn.edu](mailto:sattertt@pennmedicine.upenn.edu)



**Fig. 1 | QSIprep workflows.** QSIprep includes preprocessing (left column) and reconstruction (right column) workflows. BIDS data enter the workflow at the top left, following the blue arrow sequentially through the possible steps. The outputs from the preprocessing pipeline are inputs for the reconstruction workflows, which includes reconstruction methods from MRtrix3, DSI Studio and DIPY. A matrix of ODFs shows a fiber crossing reconstructed from multiple sampling schemes with multiple methods in QSIprep. Gray arrows labeled 'Convert formats' indicate that a reconstruction from one software package can be converted to be used in the destination software for further processing (for example, DIPY reconstructions can be used for tractography in MRtrix3). S, superior; L, left; P, posterior.

We determined significance in all tests reported here using  $t$ -statistics from a linear mixed effects model with participant as a random intercept. We estimated degrees of freedom and  $P$  values using the Satterthwaite approximation. For shelled schemes, QSIprep produced significantly less blurred images than pipelines tailored specifically for each dataset (Fig. 2a, statistical information is available in Supplementary Table 2). QSIprep images were substantially less blurred than the custom pipelines developed for the single-shell sequence from the Philadelphia Neurodevelopmental Cohort (PNC)

( $\Delta\text{FWHM} = -0.16$  mm), the multi-shell sequence from Adolescent Brain and Cognitive Development (ABCD) ( $\Delta\text{FWHM} = -0.8$  mm) and the multi-shell sequence from the Human Connectome Project (HCP)-Lifespan ( $\Delta\text{FWHM} = -0.75$  mm). Comparisons of raw and processed data further demonstrates the relatively large increase in smoothness introduced by several previously published pipelines (Extended Data Fig. 2). In contrast, the smoothness of QSIprep's outputs was slightly higher than that produced by the pipeline developed for the NODDI-optimized MultiShell 113 sequence



**Fig. 2 | QSIprep improves image quality without additional smoothing.**

**a,b.** Comparison of image smoothness (FWHM, **a**) and data quality (NDC, **b**) produced by QSIprep and previously published pipelines tailored for each acquisition scheme for shelled schemes. **c,d.** Comparison of image smoothness (**c**) and data quality (**d**) between QSIprep and raw data for nonshelled schemes (for example, Cartesian and random sampling).

( $\Delta\text{FWHM} = +0.09\text{ mm}$ ); no differences were seen in data from the Healthy Brain Network (HBN).

Notably, QSIprep yielded images with higher NDC than most of the custom pipelines we examined (Fig. 2b, statistical information is available in Supplementary Table 3). The only exception to this was the HCP pipeline, where NDC scores were not significantly different from QSIprep. These results emphasize that QSIprep produces images of superior (or at least equal) data quality compared to custom pipelines developed for a wide variety of shelled acquisition schemes.

One important advantage of QSIprep is that in addition to shelled acquisition schemes, it can also effectively process advanced nonshelled schemes using an algorithm introduced in QSIprep. In this case, direct comparisons to an existing pipeline were not available, so we only evaluated comparisons with raw data. Inevitably, any image processing introduces at least some increase in smoothness (Fig. 2c, statistical information is available in Supplementary Table 4). As expected, images processed with QSIprep were slightly but significantly smoother than the raw images ( $\Delta\text{FWHM} = +0.53\text{ mm}$ ), similar to that seen for shelled schemes (Extended Data Fig. 2). Notably, processing nonshelled sequences with QSIprep significantly improved data quality, reflected in a large increase in NDC values (Fig. 2d, statistical information is available in Supplementary Table 5).

Following preprocessing, QSIprep's set of curated reconstruction workflows provides two critical benefits to users: correct processing and a uniform derived output format. First, workflows are

designed to ensure that data preprocessed by QSIprep are handled correctly within the reconstruction workflow. Second, outputs from each reconstruction method conform to a consistent format across workflows. This emphasis on software interoperability facilitates comparisons between methods (Extended Data Fig. 3). Additionally, QSIprep allows users to apply standard processing and reconstruction methods developed for shelled sequences to advanced nonshelled sequences using a  $q$ -space-based interpolation. The ability to apply standard analytic methods to nonshelled schemes increases the accessibility of advanced nonshelled acquisition sequences.

One of the most popular applications for dMRI is to construct whole-brain structural connectomes via streamline tractography. However, file formats for storing and representing connectomes vary across software packages, thereby limiting comparisons. Furthermore, many software packages produce inconsistently sized matrices across participants, due to some participants missing small regions from high-resolution atlases. In contrast, QSIprep ensures that connectivity matrices are directly comparable across methods and participants. Specifically, the software checks that matrices are correctly shaped across all atlases and stores them in easily accessible HDF5 files. Finally, due to the interoperability of the component software elements, QSIprep allows a more diverse array of connectivity measurements to be calculated than is possible with individual software packages (Supplementary Table 1).

Several limitations of the current version of QSIprep should be noted. First, the software does not support double diffusion encoding  $q$ -space imaging or gradient tensor imaging. These scanning sequences are not widely used, are not currently supported by BIDS, and lack open preprocessing software. Second, it is critical to note that we do not claim that the reconstruction workflows are optimal for any given method, only that they implement current best practices. Traditionally, the question of optimality in reconstruction and tractography methods has been difficult to address, in part due to the lack of comparability of measures produced by different software packages. The interoperability provided by QSIprep facilitates the comparison of many measures—including orientation distribution functions (ODFs), anisotropy scalars and connectivity matrices—across reconstruction methods and sampling schemes.

Taken together, QSIprep allows researchers to correctly apply reproducible preprocessing pipelines and advanced reconstruction methods to most dMRI data: a scope currently unmatched by other dMRI pipelines (Supplementary Note 4). By harnessing cutting-edge techniques from individual software packages and unifying them in an interoperable framework, the widely generalizable methods provided by QSIprep perform as well or better than existing customized solutions that can only be applied to a subset of sampling schemes. As QSIprep's processing workflows adapt to the characteristics of the input data, it yields an appropriate pipeline as long as the user has correctly specified their data in BIDS. This alleviates much of the burden for users who wish to follow best practices in data processing, but do not have the time or skills to learn the minutiae of multiple software packages. Critically, the adaptive pipelines configured by QSIprep enhance accessibility and reproducibility without sacrificing quality. This is underscored by the result that pipelines automatically constructed by QSIprep yielded results with comparable or better data quality and smoothness compared to established pipelines for multiple studies. As such, QSIprep facilitates the adoption of fully reproducible best practices for the processing, quality assurance and reconstruction of diffusion images.

### Online content

Any methods, additional references, Nature Research reporting summaries, source data, extended data, supplementary information, acknowledgements, peer review information; details of author contributions and competing interests; and statements of

data and code availability are available at <https://doi.org/10.1038/s41592-021-01185-5>.

Received: 10 September 2020; Accepted: 17 May 2021;

Published online: 21 June 2021

## References

1. Wedeen, V. J., Hagmann, P., Tseng, W.-Y. I., Reese, T. G. & Weisskoff, R. M. Mapping complex tissue architecture with diffusion spectrum magnetic resonance imaging. *Magn. Reson. Med.* **54**, 1377–1386 (2005).
2. Alexander, D. C. A general framework for experiment design in diffusion MRI and its application in measuring direct tissue-microstructure features. *Magn. Reson. Med.* **60**, 439–448 (2008).
3. Fick, R. H. J., Wassermann, D., Caruyer, E. & Deriche, R. MAPL: tissue microstructure estimation using Laplacian-regularized MAP-MRI and its application to HCP data. *Neuroimage* **134**, 365–385 (2016).
4. Yeh, C. H., Smith, R. E., Liang, X., Calamante, F. & Connelly, A. Correction for diffusion MRI fibre tracking biases: the consequences for structural connectomic metrics. *Neuroimage* **142**, 150–162 (2016).
5. Gorgolewski, K. J. et al. The brain imaging data structure, a format for organizing and describing outputs of neuroimaging experiments. *Sci. Data* **3**, 160044 (2016).
6. Andersson, J. L. R. & Sotiropoulos, S. N. An integrated approach to correction for off-resonance effects and subject movement in diffusion MR imaging. *Neuroimage* **125**, 1063–1078 (2016).
7. Yeh, F.-C. & Tseng, W.-Y. I. NTU-90: a high angular resolution brain atlas constructed by *q*-space diffeomorphic reconstruction. *Neuroimage* **58**, 91–99 (2011).
8. Garyfallidis, E. et al. Dipy, a library for the analysis of diffusion MRI data. *Front. Neuroinform.* **8**, 8 (2014).
9. Avants, B. B., Epstein, C. L., Grossman, M. & Gee, J. C. Symmetric diffeomorphic image registration with cross-correlation: evaluating automated labeling of elderly and neurodegenerative brain. *Med. Image Anal.* **12**, 26–41 (2008).
10. Tournier, J. D. et al. MRtrix3: a fast, flexible and open software framework for medical image processing and visualisation. *NeuroImage* **202**, 116137 (2019).
11. Gorgolewski, K. J. et al. BIDS apps: improving ease of use, accessibility, and reproducibility of neuroimaging data analysis methods. *PLoS Comput. Biol.* **13**, e1005209 (2017).
12. Satterthwaite, T. D. et al. Neuroimaging of the Philadelphia Neurodevelopmental Cohort. *NeuroImage* **86**, 544–553 (2014).
13. Hagler, D. J. et al. Image processing and analysis methods for the Adolescent Brain Cognitive Development Study. *Neuroimage* **202**, 116091 (2019).
14. Pines, A. R. et al. Leveraging multi-shell diffusion for studies of brain development in youth and young adulthood. *Dev. Cogn. Neurosci.* **43**, 100788 (2020).
15. Harms, M. P. et al. Extending the Human Connectome Project across ages: imaging protocols for the Lifespan Development and Aging projects. *Neuroimage* **183**, 972–984 (2018).
16. O'Connor, D. et al. The Healthy Brain Network Serial Scanning Initiative: a resource for evaluating inter-individual differences and their reliabilities across scan conditions and sessions. *Gigascience* **6**, giw011 (2017).
17. Paquette, M., Merlet, S., Gilbert, G., Deriche, R. & Descoteaux, M. Comparison of sampling strategies and sparsifying transforms to improve compressed sensing diffusion spectrum imaging. *Magn. Reson. Med.* **73**, 401–416 (2015).
18. Yeh, F. C. et al. Differential tractography as a track-based biomarker for neuronal injury. *Neuroimage* **202**, 116131 (2019).
19. Veraart, J. et al. Denoising of diffusion MRI using random matrix theory. *Neuroimage* **142**, 394–406 (2016).
20. Fadnavis, S., Batson, J. & Garyfallidis, E. Patch2Self: denoising diffusion MRI with self-supervised learning. in *Proc. Advances in Neural Information Processing Systems* Vol. 33 (eds Larochelle, H. et al.) 16293–16303 (Curran Associates, 2020).

**Publisher's note** Springer Nature remains neutral with regard to jurisdictional claims in published maps and institutional affiliations.

© The Author(s), under exclusive licence to Springer Nature America, Inc. 2021



## Methods

**QSIprep's preprocessing workflows.** The preprocessing workflow is dynamically built based on data provided as a BIDS input. Separate dMRI scans can be grouped and processed together depending on their acquisition parameters and user-supplied options. Image processing can include denoising, Gibbs unringing, head motion, eddy current and distortion correction,  $b=0$  reference image creation (including an optional single-participant  $b=0$  template), coregistration to the T1w image, spatial normalization, image resampling and gradient rotation. The left panel in Fig. 1 depicts the sequence of these steps.

The execution of the workflow is managed by Nipype<sup>21</sup>, which provides support for multi-core parallelization, algorithm input validation and interfaces to the numerous software packages used by QSIprep. Coding style and some workflows were adapted from fMRIPrep<sup>22</sup> v1.2.6. The steps detailed in this section can be enabled or disabled by providing flags on the command-line call to QSIprep. We refer the user to the documentation at <https://qsiprep.readthedocs.io/en/latest/usage.html#command-line-arguments>.

**Conform, merge and denoise workflow.** One of the unique challenges of dMRI preprocessing is that the  $q$ -space sampling scheme is often split into multiple separate scans. Moreover, groups of these scans may be acquired with opposite phase-encoding directions so that their  $b=0$  images can be used for susceptibility distortion correction (SDC). The heuristic used by QSIprep is to divide the scans into 'warped groups' that share the same susceptibility distortions. The warped groups are sent to the conform, merge and denoise workflow.

All spatial transformation operations in QSIprep (excluding TOPUP/eddy) are performed using ANTs<sup>2</sup>. ANTs internally use an LPS+ (left-posterior-superior) coordinate system. The FSL-style bvec format required by BIDS specifies gradient directions with respect to the image axis, not world coordinates. By conforming all images and bvecs to LPS+ image orientation, ANTs can be used directly for registration and transformation on both the images and the gradient vectors. The conform step enforces this orientation and checks that the images have matching qform/sform mappings.

Next, warped groups undergo image-based artifact corrections (using MP-PCA<sup>23</sup> or Patch2Self<sup>24</sup>, Gibbs unringing<sup>24</sup>, bias correction<sup>25</sup> and  $b=0$  image-based intensity normalization) and concatenated if multiple runs are present. This step can be done as concatenate-then-denoise or denoise-then-concatenate (default), depending on the user's preference. If images are concatenated before denoising, there will be more data for MP-PCA or patch2self to include in denoising. However, if the concatenated scans are very far out of alignment with one another, the performance of MP-PCA may be suboptimal. The other denoising methods are not affected by when data are concatenated. The user can select the concatenate-then-denoise order using a command-line flag. A visual description of these workflows is presented in Supplementary Fig. 3.

**Head motion, eddy current and SDC workflow.** We combined head-motion correction (HMC), eddy current correction (ECC) and SDC into a single workflow due to the interdependence of the TOPUP and eddy tools. This workflow is split into special cases for shelled sampling schemes (multi- or single shell) and all other sampling schemes.

**Shelled sampling schemes.** If a reverse-phase-encoding direction image is available in the fmap/ or dwi/ directories, a fieldmap is calculated using TOPUP and sent to eddy to be applied in addition to HMC and ECC. In all other cases, the fieldmap is calculated using workflows adapted from fMRIPrep and applied to the motion-corrected and imputed output from eddy.

**Cartesian and random sampling schemes.** These schemes are processed using the QSIprep's SHOREline algorithm (<https://qsiprep.readthedocs.io/en/latest/preprocessing.html#head-motion-estimation-shoreline>) before being processed using the distortion correction workflows.

Regardless of the sampling schemes, SDC requires a careful selection of representative  $b=0$  images from each dMRI scan. QSIprep selects up to three (depending on availability)  $b=0$  images evenly spaced in time from each group of phase-encoding directions. Using a representative subset of all  $b=0$  images is required to limit the run time of TOPUP. The details of which images are used for SDC are included in the HTML report. Newer versions of QSIprep (0.12.0 and higher) implement the 'best  $b=0$ ' workflow used by the developmental HCP pipelines<sup>15</sup>, where  $b=0$  images are selected that have the highest average spatial correlation to the other  $b=0$  images in the same warped group.

**$b=0$  template workflow.** The reference image for each dMRI series is created by extracting the  $b=0$  images from the series after HMC, ECC and SDC. They are combined using a normalized average as implemented in ANTs and undergo a histogram equalization as implemented in DIPY. A visual report is generated showing the  $b=0$  template before and after histogram equalization.

**Intramodal template workflow.** In cases where there are multiple sessions or multiple separate dMRI scans that should not be merged, there will be multiple  $b=0$  reference images. Each can be affected by errors in SDC or intermodal coregistration to the T1w image. QSIprep provides the option to create an 'intramodal template' using ANTs template construction<sup>26</sup> on the set of  $b=0$  reference images. The intramodal template is coregistered to the T1w image instead of each individual  $b=0$  reference image. The transform to the intramodal template as well as the intramodal template's transform to the T1w image are added to the stack of transforms that get combined and applied to each dMRI (avoiding an additional interpolation).

**Coregistration and resampling workflow.** Coregistration between the  $b=0$  template image (or the intramodal  $b=0$  template) is performed using antsRegistration. If the user requests a T1w-based spatial normalization to a template, this is also performed using the antsRegistration-based workflow adapted from fMRIPrep. Similar to the HCP Pipelines<sup>27</sup> and the ABCD MMPS pipeline<sup>13</sup>, QSIprep uses a rigid transformation to register the skull-stripped T1w image to AC-PC alignment. Unlike these other pipelines, QSIprep combines all spatial transformations so that only a single resampling can be applied. However, the eddy-based workflow uses eddy's interpolation along with a separate final interpolation to AC-PC alignment. The final resampling uses a Lanczos-windowed Sinc interpolation if the requested output resolution is close to the resolution of the input data. If more than a 10% increase in spatial resolution is requested, then a BSpline interpolation is performed to prevent ringing artifact. The final resampling can at most include the affine HMC, the polynomial ECC, the nonlinear SDC, the nonlinear registration to the  $b=0$  template, the coregistration to the T1w image and the realignment to AC-PC orientation. Combining these into a single shot interpolation helps preserve high-frequency spatial features and precision of the final transform. Any T1w-based steps can be skipped using the dwi-only flag.

**QSIprep's reconstruction workflows.** A major challenge in comparing reconstruction methods is that many dMRI software packages have their own file formats, coordinate systems, orientation conventions and visualization tools (Supplementary Note 1). This diversity is compounded by the large number of possible dMRI acquisition schemes, many of which only meet the requirements of a subset of reconstruction methods. QSIprep's set of curated reconstruction workflows provides two critical benefits to users: correct processing and a uniform derived output format. First, workflows are designed to ensure that data preprocessed by QSIprep are handled correctly within the reconstruction workflow. Second, outputs from each reconstruction method conform to a consistent format across workflows.

This emphasis on software interoperability facilitates comparisons between methods. For example, Extended Data Fig. 3 displays the results from a number of reconstruction workflows, depicting disparate sampling schemes reconstructed using popular methods from MRtrix3, DSI Studio and the Laplacian-regularized mean apparent propagator MRI<sup>3</sup> implementation from DIPY. The visual similarity of the reconstructed ODFs and fiber orientation distributions (FODs) suggests that many of these methods share important features such as peak directions. All reconstruction outputs are produced in the native file format of each software package used and also consistently provided in a DSI Studio (.fib format) file.

Capitalizing on the interoperability described above, QSIprep also allows users to apply standard processing and reconstruction methods developed for shelled sequences to advanced nonshelled sequences. To do this, QSIprep converts nonshelled sampling schemes to a multi-shell scheme using a 3dSHORE-based  $q$ -space interpolation. This conversion allows, for example, the use of multi-shell multi-tissue reconstruction and MRtrix3 tractography methods on any nonshelled sampling scheme. The ability to apply standard analytic methods to nonshelled schemes increases the accessibility of these advanced acquisition sequences.

QSIprep's curated reconstruction workflows apply developer-recommended postprocessing and reconstruction steps, storing the results in both the software-native and DSI Studio formats. The pipelines were chosen from the most popular open-source diffusion imaging software packages such that there is at least one workflow for each  $q$ -space sampling scheme. A comparison of pipelines is shown in Supplementary Table 1 and their implementation details are described below grouped by software. While the included workflows use fixed parameters, users can download and edit workflow configuration files to change the workflow's behavior.

**MRtrix3.** There are a number of MRtrix3-based workflows that share the same initial steps but differ in how the FOD estimation is performed. In each MRtrix3-based workflow the fiber response function is estimated using dwi2response dhollander<sup>28</sup> with a brain mask based on the T1w. The main differences are the MRtrix3 workflows are in (1) the canonical signed digit (CSD) algorithm used to estimate white matter (WM) FODs and gray matter and cerebrospinal fluid compartments (multi-shell multi-tissue CSD, MSMT-CSD or single-shell three-tissue<sup>28</sup> CSD, SS3T-CSD) and (2) whether a T1w-based tissue segmentation is used during tractography. The \*\_noACT versions of the pipelines must be used if SDC was not performed during preprocessing. Anatomically constrained tractography (ACT) requires SDC to align the T1w-based

segmentation for accurate use during tractography. Otherwise, cropping is performed at the T1w-based gray matter-WM interface along with backtracking. In all MRtrix3 pipelines, tractography is performed using tckgen, which uses the iFOD2 probabilistic tracking method to generate  $10^7$  streamlines with a maximum length of 250 mm, minimum length of 30 mm and FOD power of 0.33. Weights for each streamline are calculated using SIFT2, which is then used to estimate the structural connectivity matrix.

**mrtrix\_multishell\_msmt.** The mrtrix\_multishell\_msmt workflow uses the dwi2fod msmt\_csd algorithm<sup>28</sup> to estimate FODs for white matter, gray matter and cerebrospinal fluid using multi-shell acquisitions. The white matter FODs are used for tractography and the T1w segmentation is used for anatomical constraints<sup>29</sup>. mrtrix\_multishell\_msmt\_noACT is identical except that no T1w-based anatomical constraints are used in tractography. mrtrix\_singleshell\_ss3t is optimized for single-shell acquisitions and also estimates multi-tissue FODs for white matter, gray matter and cerebrospinal fluid using the ss3t\_csd\_beta1 (SS3T-CSD) algorithm<sup>28</sup>, provided via the MRtrix3Tissue (<https://3Tissue.github.io>) fork of MRtrix3. The white matter FODs are used for tractography and the T1w segmentation is used for anatomical constraints<sup>29</sup>. mrtrix\_singleshell\_ss3t\_noACT removes the anatomical constraints from tractography.

**DSI Studio.** dsi\_studio\_gqi runs the standard generalized  $q$ -sampling imaging (GQI) reconstruction<sup>30</sup> followed by deterministic tractography<sup>31</sup>. GQI works on almost any sampling scheme. GQI models the diffusion ODE. Diffusion ODFs exhibit smaller peaks than are commonly seen with CSD, but robustly detect fiber crossings<sup>32</sup>. Although GQI technically works on diffusion tensor imaging (DTI) scans, with spherical sampling on a single shell around  $b = 1,000 \text{ s mm}^{-2}$ , its performance markedly improves when more  $q$ -space samples are available. The tractography performed in this pipeline ensures that 5 million streamlines are created with a maximum length of 250 mm, a minimum length of 30 mm, random seeding, a step size of 1 mm and an automatically calculated quantitative anisotropy<sup>31</sup> threshold. Additionally, a number of anisotropy scalar images are produced such as quantitative anisotropy<sup>30</sup>, generalized fractional anisotropy and the isotropic component of the ODE.

**DIPY.** *dipy\_mapmri.* Mean apparent propagator MRI is a reconstruction method<sup>33</sup> that can estimate ensemble average diffusion propagators (EAPs) and ODFs analytically using multi-shell, Cartesian or random  $q$ -space sampling schemes. This method produces EAP-derived scalars such as return to origin probability, return to axis probability, return to plane probability,  $q$ -space inverse variance and mean-squared displacement. The ODFs are saved in DSI Studio format and optionally as spherical harmonics coefficients in the MRtrix3 format. *dipy\_3dshore.* The 3D Simple Harmonic Oscillator-based Reconstruction and Estimation (3dSHORE)<sup>34</sup> method also uses a closed-form solution to estimate EAPs and ODFs from  $q$ -space data. This workflow uses the BrainSuite 3dSHORE basis in a DIPY reconstruction. Much like dipy\_mapmri, EAP-related scalars such as return to origin probability, return to axis probability, return to plane probability and mean-squared displacement are estimated. For both of these reconstruction pipelines, tractography is run identically to the dsi\_studio\_gqi.

**Experimental DSI scheme-converting reconstruction.** csds\_i\_3dshore. This pipeline is for DSI or compressed-sensing DSI. The first step is an L2-regularized 3dSHORE reconstruction<sup>3</sup> of the ensemble average propagator in each voxel. These EAPs are then used to (1) calculate ODFs, which are then sent to DSI Studio for tractography and (2) impute signal for a multi-shell (specifically HCP) sampling scheme, which is run through the mrtrix\_multishell\_msmt pipeline. The resampling is similar to a previously described GQI-based method<sup>35</sup> but uses the 3dSHORE basis set to estimate out-of-sample images.

**Structural connectivity matrices.** Tractography resulting in connectivity matrices are conformed to a standard HDF5-based output format so as to be directly comparable across methods and software packages. A set of commonly used parcellation schemes are included with QSIprep, such as the Schaefer atlases in the 100, 200 and 400 parcel resolutions, the brainnetome atlas (264 regions)<sup>36</sup>, AICHA (384 regions)<sup>37</sup>, Gordon (333 regions)<sup>38</sup>, the AAL (116 regions)<sup>39</sup> and the Power atlas (264 regions)<sup>40</sup>. Furthermore, users can easily add their own custom atlases as required.

**Evaluation data.** Data were gathered from a number of independent studies from multiple institutions. Each study obtained informed consent from participants and was approved by their institutions' ethics committees. These samples were selected to test a variety of  $q$ -space sampling schemes and evaluate if QSIprep handles each one correctly. An overview of the acquisition parameters is provided in Extended Data Fig. 1. QSIprep was run on the raw data from each study. Spatial smoothness and NDC<sup>18</sup> were calculated for the QSIprep-preprocessed data and for the data processed using a pipeline specifically designed for that sampling scheme. In the case of nonshelled schemes, QSIprep was compared to unprocessed data.

**Single-shell, DTI.** The single-shell data were collected as part of the PNC<sup>12</sup> and processed according to previously described methods<sup>41</sup>. This pipeline is similar

to QSIprep, using eddy (from FSL5) and custom code for applying distortion correction. The QSIprep pipeline differs in that it adds MP-PCA, Gibbs unringing, FSL6 and resampling using ANTs. A total of 111 participants were randomly selected from the available PNC dMRI data.

**Multi-shell, NODDI-optimized.** This sampling scheme was designed with the goal of fitting microstructural models such as NODDI<sup>42</sup>. The published data<sup>44</sup> used FSL5's TOPUP and eddy with outlier replacement enabled for preprocessing. The QSIprep pipeline differed in that it added MP-PCA denoising, Gibbs unringing, FSL6 and resampling using ANTs. We evaluated a sample of 136 participants.

**Multi-shell, ABCD.** A total of 106 datasets were downloaded from the National Institute of Mental Health (NIMH) Data Archive repository as raw .NIfTI files and following minimal preprocessing. The ABCD dMRI preprocessing pipeline<sup>13</sup> does not use any of the same software as QSIprep but performs similar steps. The ABCD pipeline includes gradient nonlinearity correction and uses in-house code for performing eddy current and distortion correction. QSIprep adds MP-PCA, Gibbs unringing, ECC, SDC using FSL6 and resampling using ANTs.

**Multi-shell, HCP-Lifespan.** A total of 34 participants were scanned using the HCP-Lifespan imaging protocol<sup>15</sup> and processed using both the official HCP diffusion pipelines<sup>43</sup> (v4.0.0-alpha.5) and QSIprep. The HCP diffusion pipeline included motion and ECC, distortion correction, across-scan intensity normalization, coregistration to the T1w image, gradient unwarping and image pair averaging. QSIprep was upgraded as part of 0.9.0beta1 to include the image pair averaging so that QC measures could be compared directly between the QSIprep and HCP pipeline outputs. QSIprep was adjusted to use a quadratic first-level model in eddy to match the HCP diffusion pipeline.

**Multi-shell, HBN.** A total of 27 HBN<sup>16</sup> participants were processed using both an early prototype version of dMRIprep (<https://github.com/nipy/dmriprep>) and QSIprep. Both dMRIprep and QSIprep use TOPUP and eddy for distortion, eddy current and motion correction, but dMRIprep did not include Gibbs unringing or MP-PCA.

**Cartesian grid (DSI) schemes.** Before QSIprep, there was no publicly available software for applying HMC to DSI or CS-DSI acquisitions. Therefore, the QSIprep-preprocessed images were compared directly to the NDC calculated on the raw images. DSI258 was a repeated measures study with eight repeated scans per participant. CS-DSI acquired four different random schemes per participant. DSI789 scans acquired 789 unique coordinates on a Cartesian grid in  $q$ -space.

**Ethics oversight.** No new data were collected specifically for this study. All other data were acquired with IRB approval at their original institutions and informed consent from participants. The University of Pennsylvania IRB approved DTI64 (810336), HCP-Lifespan (819931), MultiShell113 (822831), CS-DSI (829744) and DSI789 (828062). DSI258 was approved by the Institutional Review Board at the University of California Santa Barbara (23-17-0532). ABCD and HBN datasets are publicly available, deidentified data resources collected as part of large consortia.

**Reporting Summary.** Further information on research design is available in the Nature Research Reporting Summary linked to this article.

## Data availability

Source data for Fig. 2 and Supplementary Tables 1–4 are available at [https://pennlinc.github.io/qsiprep\\_paper/](https://pennlinc.github.io/qsiprep_paper/) (DOI 10.5281/zenodo.4667846). In addition, source data for Fig. 2 and Extended Data Fig. 2 are provided with this paper. Most imaging data are available from public repositories. PNC data (DTI64) are available on dbGAP ([https://www.ncbi.nlm.nih.gov/projects/gap/cgi-bin/study.cgi?study\\_id=phs000607.v3.p2](https://www.ncbi.nlm.nih.gov/projects/gap/cgi-bin/study.cgi?study_id=phs000607.v3.p2)). ABCD data are publicly available in both raw BIDS ([https://nda.nih.gov/edit\\_collection.html?id=3165](https://nda.nih.gov/edit_collection.html?id=3165)) and preprocessed ([https://nda.nih.gov/edit\\_collection.html?id=2573](https://nda.nih.gov/edit_collection.html?id=2573)) states. HBN data are available on the NeuroImaging Tools and Resources Collaboratory ([https://fcon\\_1000.projects.nitrc.org/indi/cmi\\_healthy\\_brain\\_network/sharing\\_neuro.html](https://fcon_1000.projects.nitrc.org/indi/cmi_healthy_brain_network/sharing_neuro.html)) under a data use agreement. Other imaging datasets did not obtain explicit participant consent for data to be placed in a public repository. HCP-Lifespan imaging data are available on request to G.K.A. DSI258 is available on request to J.M.V. DSI 756 is available on request to D.S.B. CS-DSI and MultiShell 113 are available on request to T.D.S. Source data are provided with this paper.

## Code availability

All code used to perform the statistical tests are available at: [https://pennlinc.github.io/qsiprep\\_paper/](https://pennlinc.github.io/qsiprep_paper/) (ref. 44) and the QSIprep source code is available at [github.com/pennlinc/qsiprep](https://github.com/pennlinc/qsiprep). Docker images for the versions of QSIprep used in this paper are available on DockerHub at v0.8.0 and 0.9.0beta1. Newer versions are available. A compute capsule containing QSIprep and example data is available on Code Ocean<sup>45</sup>.

## References

21. Gorgolewski, K. et al. Nipype: a flexible, lightweight and extensible neuroimaging data processing framework in Python. *Front. Neuroinform.* **5**, <https://doi.org/10.3389/fninf.2011.00013> (2011).
22. Esteban, O. et al. fMRIPrep: a robust preprocessing pipeline for functional MRI. *Nat. Methods* **16**, 111–116 (2019).
23. Veraart, J., Sijbers, J., Sunaert, S., Leemans, A. & Jeurissen, B. Weighted linear least squares estimation of diffusion MRI parameters: Strengths, limitations, and pitfalls. *Neuroimage* **81**, 335–346 (2013).
24. Kellner, E., Dhital, B., Kiselev, V. G. & Reiser, M. Gibbs-ringing artifact removal based on local subvoxel-shifts. *Magn. Reson. Med.* **76**, 1574–1581 (2016).
25. Tustison, N. J. et al. N4ITK: improved N3 bias correction. *IEEE Trans. Med. Imaging* **29**, 1310–1320 (2010).
26. Avants, B. B. et al. The optimal template effect in hippocampus studies of diseased populations. *Neuroimage* **49**, 2457–2466 (2010).
27. Sotiropoulos, S. N. et al. Advances in diffusion MRI acquisition and processing in the Human Connectome Project. *Neuroimage* **80**, 125–143 (2013).
28. Dhollander, T., Raffelt, D. & Connelly, A. Unsupervised 3-tissue response function estimation from single-shell or multi-shell diffusion MR data without a co-registered T1 image. in *Proc. ISMRM Workshop on Breaking the Barriers of Diffusion MRI* **5** (2016).
29. Smith, R. E., Tournier, J. D., Calamante, F. & Connelly, A. Anatomically-constrained tractography: improved diffusion MRI streamlines tractography through effective use of anatomical information. *Neuroimage* **62**, 1924–1938 (2012).
30. Yeh, F.-C., Wedeen, V. J. & Tseng, W.-Y. I. Generalized  $q$ -sampling imaging. *IEEE Trans. Med. Imaging* **29**, 1626–1635 (2010).
31. Yeh, F. C., Verstynen, T. D., Wang, Y., Fernández-Miranda, J. C. & Tseng, W. Y. I. Deterministic diffusion fiber tracking improved by quantitative anisotropy. *PLoS ONE* **8**, e80713 (2013).
32. Yeh, F. C., Wedeen, V. J. & Tseng, W. Y. I. Practical crossing fiber imaging with combined DTI datasets and generalized reconstruction algorithm. in *Proc. Intl Soc. Magnetic Resonance Med.* 365 (2009).
33. Özarslan, E. et al. Mean apparent propagator (MAP) MRI: a novel diffusion imaging method for mapping tissue microstructure. *Neuroimage* **78**, 16–32 (2013).
34. Özarslan, E., Koay, C. G. & Basser, P. J. in *Applied and Numerical Harmonic Analysis* (eds Özarslan, E. et al.) 373–399 (Springer International Publishing, 2013).
35. Yeh, F.-C. & Verstynen, T. D. Converting multi-shell and diffusion spectrum imaging to high angular resolution diffusion imaging. *Front. Neurosci.* **10**, 418 (2016).
36. Fan, L. et al. The Human Brainnetome Atlas: a new brain atlas based on connective architecture. *Cereb. Cortex* **26**, 3508–3526 (2016).
37. Joliot, M. et al. AICHA: an atlas of intrinsic connectivity of homotopic areas. *J. Neurosci. Methods* **254**, 46–59 (2015).
38. Gordon, E. M. et al. Generation and evaluation of a cortical area parcellation from resting-state correlations. *Cereb. Cortex* **26**, 288–303 (2016).
39. Tzourio-Mazoyer, N., Landeau, B. & Papathanassiou, D. Automated anatomical labeling of activations in SPM using a macroscopic anatomical parcellation of the MNI MRI single-subject brain. *Neuroimage* **15**, 273–289 (2002).
40. Power, J. D., Fair, D. A. & Schlaggar, B. L. Development of human functional brain networks. *Neuron* **67**, 735–748 (2010).
41. Roalf, D. R. et al. The impact of quality assurance assessment on diffusion tensor imaging outcomes in a large-scale population-based cohort. *Neuroimage* **125**, 903–919 (2016).
42. Zhang, H., Schneider, T., Wheeler-Kingshott, C. A. & Alexander, D. C. NODDI: practical in vivo neurite orientation dispersion and density imaging of the human brain. *Neuroimage* **61**, 1000–1016 (2012).
43. Glasser, M. F. et al. The minimal preprocessing pipelines for the Human Connectome Project. *Neuroimage* **80**, 105–124 (2013).
44. Cieslak, M. PennLINC/qsiprep\_paper: Publication Version. Zenodo <https://doi.org/10.5281/zenodo.4667846> (2021)
45. Cieslak, M. et al. (2021) QSIprep: An integrative platform for preprocessing and reconstructing diffusion MRI data [Source Code]. <https://doi.org/10.24433/CO.6311778.v1> (2021).

## Acknowledgements

Funding came from the following: grant nos. R01 MH11886 for D.J.O., D.S.B. and T.D.S., NICHD R01HD09586101 to J.D.Y., NINDS R01-NS099348-01 for X.H. and D.S.B., UL1TR001878 for J.D. and M.B.K., 1 U01 EY025864-01 to G.K.A., P30 EY001583 to the Vision Research Center, MH080243 and Staunton Farm Foundation for B.S.L., T32 MH 018951 for L.M.C., R01MH113550, RF1MH116920, R01MH120482 for T.D.S., CBICA Software Seed grants for M.C. and A.A., no. R01-EB027585-01 for E.G., S.F., A.R., A.H.R. and A.K., W911NF-16-1-0474 from the Army Research Office and by the Institute for Collaborative Biotechnologies under Cooperative Agreement no. W911NF-19-2-0026 with the Army Research Office to S.T.G. and J.M.V., RF1AG054409 to C.D. B.S.L. was supported by grant no. T32MH014654. Support for the collection of the data for Philadelphia Neurodevelopment Cohort (PNC) was provided by grant no. RC2MH089983 awarded to R.E.G. Data used in the preparation of this article were obtained from the ABCD Study (<https://abcdstudy.org>), held in the NIMH Data Archive. This is a multisite, longitudinal study designed to recruit more than 10,000 children age 9–10 years and follow them over 10 years into early adulthood. The ABCD Study is supported by the National Institutes of Health and additional federal partners under award numbers U01DA041048, U01DA050989, U01DA051016, U01DA041022, U01DA051018, U01DA051037, U01DA050987, U01DA041174, U01DA041106, U01DA041117, U01DA041028, U01DA041134, U01DA050988, U01DA051039, U01DA041156, U01DA041025, U01DA041120, U01DA051038, U01DA041148, U01DA041093, U01DA041089, U24DA041123 and U24DA041147. A full list of supporters is available at <https://abcdstudy.org/federal-partners.html>. A listing of participating sites and a complete listing of the study investigators can be found at [https://abcdstudy.org/consortium\\_members/](https://abcdstudy.org/consortium_members/). ABCD consortium investigators designed and implemented the study and/or provided data but did not necessarily participate in analysis or writing of this report. This paper reflects the views of the authors and may not reflect the opinions or views of the National Institutes of Health or ABCD consortium investigators.

## Author contributions

M.C., P.A.C., X.H., F.-C.Y., T.D., A.A., M.A.E., S.F., W.F., E.G., A.K., A.R.-H., J.B., L.M.C., P.F., T.M.T., A.P.M., V.J.S., U.A.T., J.D.Y., S.T.G. and T.D.S. developed QSIprep by code contribution, testing and documentation. Data were collected, curated and shared by G.K.A., D.S.B., R.F.B., C.D., J.A.D., E.E., D.A.F., B.G., R.C.G., R.E.G., M.B.K., B.S.L., A.P.M., M.P.M., D.J.O., A.P., A.R., J.M.V. and S.T.G. Preprocessing pipelines (scheme-specific or QSIprep) were run and shared by G.K.A., R.F.B., J.B., P.F., A.K., A.R.P., D.R.R., A.R.-H. and A.R. Statistical tests were designed and implemented by M.C., B.S.L., T.M.T. and T.D.S.

## Competing interests

The authors declare no competing interests.

## Additional information




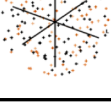

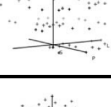
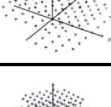
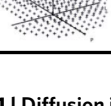
**Extended data** is available for this paper at <https://doi.org/10.1038/s41592-021-01185-5>.

**Supplementary information** The online version contains supplementary material available at <https://doi.org/10.1038/s41592-021-01185-5>.

**Correspondence and requests for materials** should be addressed to M.C. or T.D.S.

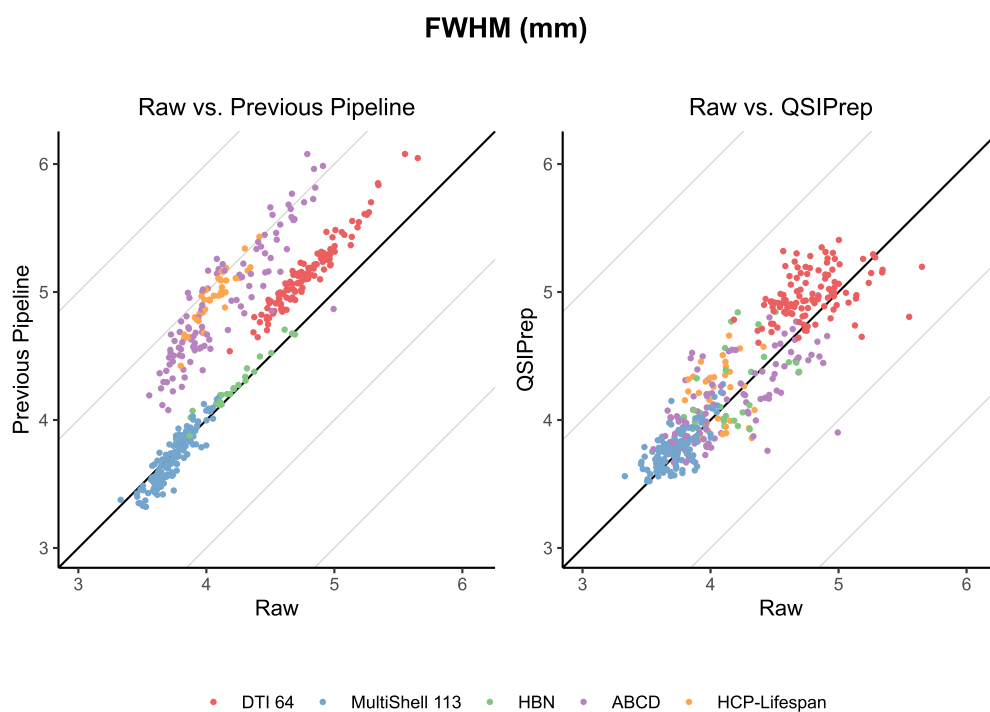
**Peer review information** *Nature Methods* thanks Jonathan D. Clayden and the other, anonymous, reviewer(s) for their contribution to the peer review of this work. Nina Vogt was the primary editor on this article and managed its editorial process and peer review in collaboration with the rest of the editorial team.

**Reprints and permissions information** is available at [www.nature.com/reprints](http://www.nature.com/reprints).

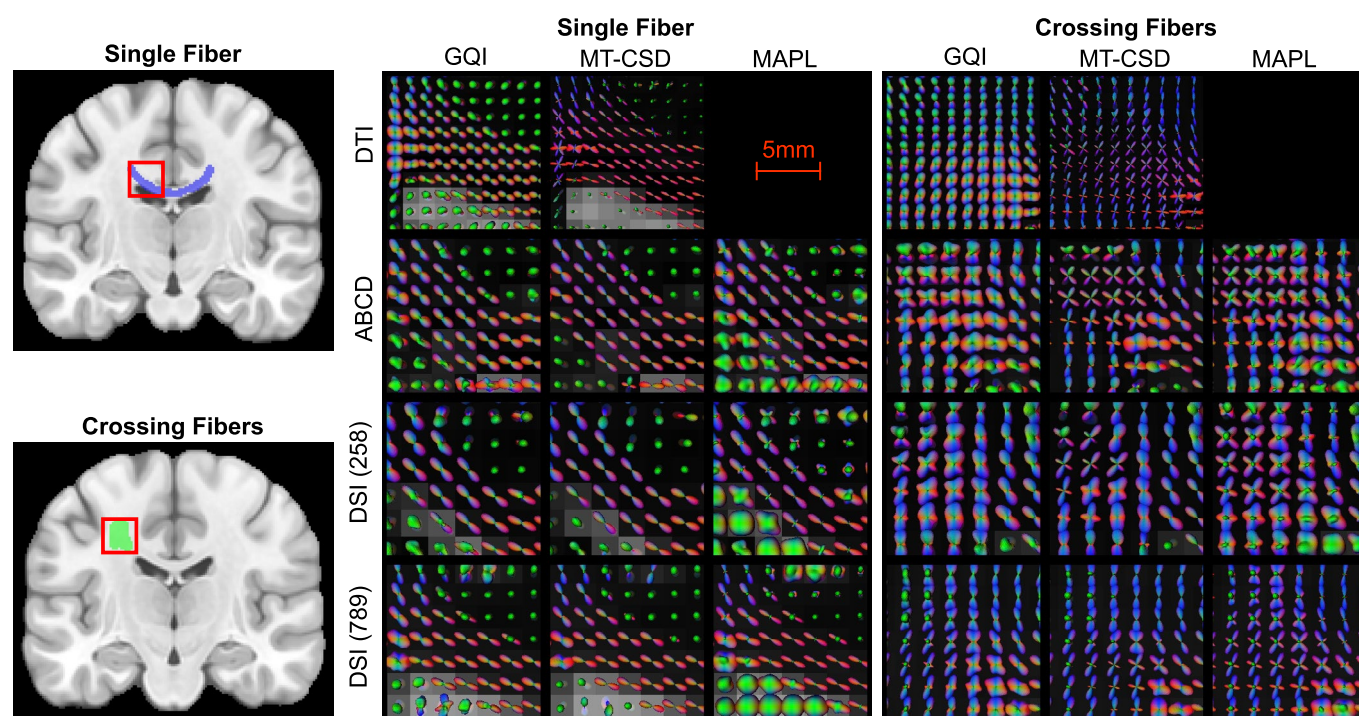
	Scheme	Scheme Category	# Directions	Max $b$ ( $s/mm^2$ )	Voxel Size (mm)	# Scans	Age (years) / Gender	Pipeline Citation
DTI 64		DTI	64	1000	2	111	15 ± 3.6 54% F	35
MultiShell 113		Multi-shell	113	3000	1.7	135	21 ± 3.5 57% F	37
ABCD		Multi-shell	103	3000	1.7	106	9.9 ± 0.6 46% F	26
HCP-Lifespan		Multi-shell	199	3000	1.5	34	27.7 ± 9 47% F	23
HBN		Multi-shell	129	3000	1.7	27	10 ± 2.8 44% F	39
CS-DSI		Random	55, 57, 92	5000	1.7	79	26.5 ± 5.1 50% F	N/A
DSI 258		DSI	258	5000	2.0	150	22 ± 3.5 63% F	N/A
DSI 789		DSI	789	5000	2.0	13	23.8 ± 5.1 69% F	N/A

**Extended Data Fig. 1 | Diffusion imaging data used in QSIprep development and evaluation.** Cartesian (DSI), random (CS-DSI), and shelled (single-shell DTI and multi-shell) sequences were used to test the preprocessing and reconstruction workflows in QSIprep. Sequences varied widely in their maximum  $b$ -value (1000–5000  $s/mm^2$ ), number of  $q$ -space samples (64–789) and voxel size (1.5–2.3 mm). The row colors represent these schemes across all figures. The colors in the HCP-Lifespan image indicate that these samples came from different scans, grouped by phase-encoding direction.





**Extended Data Fig. 2 | Comparing added smoothness from QSIPrep and previous pipelines.** Preprocessing generally increases the spatial smoothness of images relative to the raw images. Here the raw image smoothness (x-axis) is compared to the same images after being processed by the published pipeline for each dataset (left) and QSIPrep (right). The direct comparison between QSIPrep and the Previous Pipeline is presented in Fig. 2.



**Extended Data Fig. 3 | QSIprep reconstruction workflows produce comparable output across diverse sampling schemes and reconstruction methods.**

Four sampling schemes each reconstructed using four methods: GQI from DSI Studio, multi-tissue CSD from MRtrix, and MAPL from Dipy. ODF fields are shown in two white matter regions (left), a single fiber area in the corpus callosum (top) and a crossing fiber region in the centrum semiovale (bottom). The middle panel shows ODFs reconstructed in the single fiber region, and the right panel shows ODFs reconstructed in the crossing fiber region for the four sampling schemes (rows) and the three reconstruction methods (columns).

## Reporting Summary

Nature Research wishes to improve the reproducibility of the work that we publish. This form provides structure for consistency and transparency in reporting. For further information on Nature Research policies, see our [Editorial Policies](#) and the [Editorial Policy Checklist](#).

### Statistics

For all statistical analyses, confirm that the following items are present in the figure legend, table legend, main text, or Methods section.

- | n/a                                 | Confirmed  |
|-------------------------------------|--|
| <input type="checkbox"/>            | <input checked="" type="checkbox"/> The exact sample size ( $n$ ) for each experimental group/condition, given as a discrete number and unit of measurement  |
| <input type="checkbox"/>            | <input checked="" type="checkbox"/> A statement on whether measurements were taken from distinct samples or whether the same sample was measured repeatedly  |
| <input type="checkbox"/>            | <input checked="" type="checkbox"/> The statistical test(s) used AND whether they are one- or two-sided<br><i>Only common tests should be described solely by name; describe more complex techniques in the Methods section.</i>   |
| <input type="checkbox"/>            | <input checked="" type="checkbox"/> A description of all covariates tested   |
| <input type="checkbox"/>            | <input checked="" type="checkbox"/> A description of any assumptions or corrections, such as tests of normality and adjustment for multiple comparisons  |
| <input type="checkbox"/>            | <input checked="" type="checkbox"/> A full description of the statistical parameters including central tendency (e.g. means) or other basic estimates (e.g. regression coefficient) AND variation (e.g. standard deviation) or associated estimates of uncertainty (e.g. confidence intervals) |
| <input type="checkbox"/>            | <input checked="" type="checkbox"/> For null hypothesis testing, the test statistic (e.g. $F$ , $t$ , $r$ ) with confidence intervals, effect sizes, degrees of freedom and $P$ value noted<br><i>Give <math>P</math> values as exact values whenever suitable.</i>                            |
| <input checked="" type="checkbox"/> | <input type="checkbox"/> For Bayesian analysis, information on the choice of priors and Markov chain Monte Carlo settings  |
| <input checked="" type="checkbox"/> | <input type="checkbox"/> For hierarchical and complex designs, identification of the appropriate level for tests and full reporting of outcomes  |
| <input checked="" type="checkbox"/> | <input type="checkbox"/> Estimates of effect sizes (e.g. Cohen's $d$ , Pearson's $r$ ), indicating how they were calculated  |

*Our web collection on [statistics for biologists](#) contains articles on many of the points above.*

### Software and code

Policy information about [availability of computer code](#)

Data collection No data was specifically collected for this study.

Data analysis A docker image containing the software and all dependencies is available at <https://hub.docker.com/r/pennnbl/qsiprep>. Source code for preprocessing is available at [github.com/pennnbl/qsiprep](https://github.com/pennnbl/qsiprep) and statistical analyses of NDC and FWHM are available at [github.com/pennnbl/qsiprep\\_paper](https://github.com/pennnbl/qsiprep_paper).

Specific software versions used in QSIPrep were:

Neuroimaging Software:

FSL==6.0.3  
AFNI==Jun 12 2017 (Version Debian-16.2.07~dfsg.1-5~nd16.04+1)  
freesurfer==Linux-centos6\_x86\_64-stable-pub-v6.0.1-f53a55a  
bids-validator==1.2.3  
c3d==unversioned, nightly build 9/23/2020

Compiled from source at the following commit:

DSI Studio==eb8433e8923d4bb26bd6ee04d0da4bdede55ed85  
MRtrix3==5d6b3a6ffc6ee651151779539c8fd1e2e03fad81  
MRtrix 3Tissue==c1367255f51a3cbe774c8317448cdc0b0aa587be  
ANTs==e00e8164d7a92f048e5d06e388a15c1ee8e889c4

Python libraries:

bids-validator==1.5.7

boto==2.49.0  
cached-property==1.5.2  
certifi==2020.6.20  
cffi==1.11.5  
chardet==3.0.4  
ci-info==0.2.0  
citeproc-py==0.5.1  
click==7.1.2  
codecov==2.1.10  
conda==4.5.12  
coverage==5.3  
cryptography==2.4.2  
cyclr==0.10.0  
Cython==0.29.2  
cytoolz==0.11.0  
datalad==0.13.5  
decorator==4.4.2  
defusedxml==0.6.0  
Deprecated==1.2.10  
dipy==1.3.0  
docopt==0.6.2  
docutils==0.16  
duecredit==0.8.0  
entrypoints==0.3  
etelemetry==0.2.2  
fasteners==0.15  
filelock==3.0.12  
fury==0.5.1  
future==0.18.2  
h5py==3.1.0  
humanize==3.1.0  
idna==2.8  
imageio==2.5.0  
imagesize==1.2.0  
importlib-metadata==2.0.0  
indexed-gzip==1.3.2  
iniconfig==1.1.1  
ipython-genutils==0.2.0  
iso8601==0.1.13  
isodate==0.6.0  
jeepney==0.4.3  
Jinja2==2.11.2  
joblib==0.17.0  
jsmin==2.2.2  
jsonschema==3.2.0  
jupyter-client==6.1.7  
jupyter-core==4.6.3  
jupyterlab-pygments==0.1.2  
keyring==21.4.0  
keyrings.alt==4.0.1  
kiwisolver==1.2.0  
lxml==4.6.1  
MarkupSafe==1.1.1  
matplotlib==2.2.3  
mistune==0.8.4  
mkl-fft==1.2.0  
mkl-random==1.1.1  
mkl-service==2.3.0  
monotonic==1.5  
msgpack==1.0.0  
nbclient==0.5.1  
nbconvert==6.0.7  
nbformat==5.0.8  
nbsphinx==0.8.0  
nest-asyncio==1.4.2  
nibabel==3.2.0  
nilearn==0.6.2  
nipype==1.5.1  
num2words==0.5.10  
numpy==1.18.5  
olefile==0.46  
packaging==20.4  
pandas==0.24.0  
pandocfilters==1.4.3  
patool==1.12  
patsy==0.5.1



```

Pillow==6.0.0
pluggy==0.13.1
prov==2.0.0
psutil==5.7.3
py==1.9.0
pybids==0.9.5
pycosat==0.6.3
pyparser==2.19
pydot==1.4.1
pydotplus==2.0.2
PyGithub==1.53
Pymments==2.7.2
PyJWT==1.7.1
pyOpenSSL==18.0.0
pyparsing==2.4.7
pysistent==0.17.3
PySocks==1.6.8
pytest==6.1.2
python-dateutil==2.8.1
pytz==2020.1
PyYAML==5.3.1
pymq==19.0.2
qsimprep 0.8.0, 0.9.1beta1
rdflib==5.0.0
requests==2.21.0
ruamel-yaml==0.15.46
scikit-image==0.14.2
scikit-learn==0.20.2
scipy==1.2.0
seaborn==0.9.0
SecretStorage==3.1.2
sentry-sdk==0.19.2
SHORELine==0.6.3
SimpleITK==2.0.1
simplejson==3.17.2
six==1.15.0
sklearn==0.0
snowballstemmer==2.0.0
Sphinx==2.2.0
sphinx-argparse==0.2.5
sphinx-rtd-theme==0.5.0
sphinxcontrib-applehelp==1.0.2
sphinxcontrib-devhelp==1.0.2
sphinxcontrib-htmlhelp==1.0.3
sphinxcontrib-jsmath==1.0.1
sphinxcontrib-qthelp==1.0.3
sphinxcontrib-serializinghtml==1.1.4
SQLAlchemy==1.3.20
svgutils==0.3.1
testpath==0.4.4
toml==0.10.2
tornado==6.0.4
tqdm==4.51.0
traitlets==5.0.5
traits==4.6.0
urllib3==1.24.1
vtk==8.1.2
webencodings==0.5.1
Whoosh==2.7.4
wrapt==1.12.1
xvfbwrapper==0.2.9
zipp==3.4.0

```

For manuscripts utilizing custom algorithms or software that are central to the research but not yet described in published literature, software must be made available to editors and reviewers. We strongly encourage code deposition in a community repository (e.g. GitHub). See the Nature Research [guidelines for submitting code & software](#) for further information.

## Data

Policy information about [availability of data](#)

All manuscripts must include a [data availability statement](#). This statement should provide the following information, where applicable:

- Accession codes, unique identifiers, or web links for publicly available datasets
- A list of figures that have associated raw data
- A description of any restrictions on data availability

Source data for Figure 2 and Supplementary Tables 1-4 are available at [https://pennlinc.github.io/qsiprep\\_paper/](https://pennlinc.github.io/qsiprep_paper/) (DOI: 10.5281/zenodo.4667846). Imaging data is available with restrictions depending on the original source of the data. PNC data is available on dbGAP [[https://www.ncbi.nlm.nih.gov/projects/gap/cgi-bin/study.cgi?study\\_id=phs000607.v3.p2](https://www.ncbi.nlm.nih.gov/projects/gap/cgi-bin/study.cgi?study_id=phs000607.v3.p2)]. ABCD data is publicly available in both raw BIDS ([https://nda.nih.gov/edit\\_collection.html?id=3165](https://nda.nih.gov/edit_collection.html?id=3165)) and preprocessed ([https://nda.nih.gov/edit\\_collection.html?id=2573](https://nda.nih.gov/edit_collection.html?id=2573)) states. HBN data is available on the NeuroImaging Tools and Resources Collaboratory (NITRC [[http://fcon\\_1000.projects.nitrc.org/indi/healthy\\_brain\\_network/sharing\\_neuro.html](http://fcon_1000.projects.nitrc.org/indi/healthy_brain_network/sharing_neuro.html)]) under a data use agreement. HCP-Lifespan imaging data is available upon request to GKA. DSI 258 is available upon request to JMV. DSI 756 is available upon request to DSB. CS-DSI, DTI64 and MultiShell113 are available upon request to TDS.

## Field-specific reporting

Please select the one below that is the best fit for your research. If you are not sure, read the appropriate sections before making your selection.

- ☒ Life sciences ☐ Behavioural & social sciences ☐ Ecological, evolutionary & environmental sciences

For a reference copy of the document with all sections, see [nature.com/documents/nr-reporting-summary-flat.pdf](https://nature.com/documents/nr-reporting-summary-flat.pdf)

## Life sciences study design

All studies must disclose on these points even when the disclosure is negative.

Sample size	The total number of acquisitions analyzed was 657. For studies with less than 1000 acquisitions, the entire study's data was used (MultiShell 113, CS-DSI, HCP-Lifespan, DSI 258, DSI 789). The HBN number was limited by the number of available preprocessed images using the previous pipeline. The ABCD subjects were chosen based on who had available minimally preprocessed data on NDA and BIDS-curated data. DTI 64 subjects were randomly selected from the PNC cohort to approximately match the number of subjects in MultiShell 113 and ABCD.
Data exclusions	No data were purposely excluded from analysis. Two subjects from HCP-Lifespan failed BIDS curation and were not processed, resulting in a total of 34. One subject from CS-DSI and one subject from MultiShell113 also had insufficient BIDS data resulting in totals of 79 and 135 total subjects respectively.
Replication	Statistical analyses were run in two separate computing environments using data and code directly downloaded from <a href="https://github.com/pennlinc/qsiprep_paper">github.com/pennlinc/qsiprep_paper</a> . All processing was done using a containerized pipeline.
Randomization	Participants were not divided into separate experimental groups. All scans were processed through both the previous acquisition-specific pipeline and QSIprep.
Blinding	Participants were not divided into separate experimental groups.

## Reporting for specific materials, systems and methods

We require information from authors about some types of materials, experimental systems and methods used in many studies. Here, indicate whether each material, system or method listed is relevant to your study. If you are not sure if a list item applies to your research, read the appropriate section before selecting a response.

### Materials & experimental systems

n/a	Involved in the study
<input checked="" type="checkbox"/>	<input type="checkbox"/> Antibodies
<input checked="" type="checkbox"/>	<input type="checkbox"/> Eukaryotic cell lines
<input checked="" type="checkbox"/>	<input type="checkbox"/> Palaeontology and archaeology
<input checked="" type="checkbox"/>	<input type="checkbox"/> Animals and other organisms
<input type="checkbox"/>	<input checked="" type="checkbox"/> Human research participants
<input checked="" type="checkbox"/>	<input type="checkbox"/> Clinical data
<input checked="" type="checkbox"/>	<input type="checkbox"/> Dual use research of concern

### Methods

n/a	Involved in the study
<input checked="" type="checkbox"/>	<input type="checkbox"/> ChIP-seq
<input checked="" type="checkbox"/>	<input type="checkbox"/> Flow cytometry
<input type="checkbox"/>	<input checked="" type="checkbox"/> MRI-based neuroimaging

## Human research participants

Policy information about [studies involving human research participants](#)

Population characteristics	Age, gender and phenotypic data were not immediately available for all cases and were not used as a criteria for inclusion or exclusion in the study.
Recruitment	No subjects were recruited for this study. All data comes from previous studies or public repositories.
Ethics oversight	No new data was collected specifically for this study. All other data was acquired with IRB approval at their original institutions and informed consent from participants. The University of Pennsylvania IRB approved DTI 64 (810336), HCP-Lifespan (819931), MultiShell 113 (822831), CS-DSI (829744), DSI 789 (828062). DSI258 was approved by the Institutional Review Board at the University of California Santa Barbara (23-17-0532). ABCD and HBN datasets are publicly available, de-identified data resources collected as part of large consortia.

Note that full information on the approval of the study protocol must also be provided in the manuscript.

## Magnetic resonance imaging

### Experimental design

Design type	Diffusion imaging
Design specifications	Each session acquired one or more dMRI acquisitions and at least one T1-weighted anatomical acquisition.
Behavioral performance measures	No behavioral tasks are included in this study.

### Acquisition

Imaging type(s)	Structural, diffusion, fieldmap
Field strength	3
Sequence & imaging parameters	Eight different image acquisition parameter sets were investigated in this study. They are detailed in Extended Data Figure 4 and Online Methods.
Area of acquisition	Whole Brain
Diffusion MRI	<input checked="" type="checkbox"/> Used <input type="checkbox"/> Not used
Parameters	Number of directions, b-values varied across acquisitions. See Extended Data Figure 4

### Preprocessing

Preprocessing software	Data were preprocessed using QSIprep versions 0.8.0 or 0.9.0beta1 using default parameters.
Normalization	Spatial normalization is available in QSIprep but not used for any results reported here.
Normalization template	Normalization was not used for any results reported here.
Noise and artifact removal	Noise and artifact removal differed depending on the pipeline being run. This is detailed in the Online Methods section.
Volume censoring	No volumes were censored

### Statistical modeling & inference

Model type and settings	Each DWI acquisition produced a single value for FWHM and a single value for NDC for each pipeline. These were compared using a Linear Mixed Effects model.
Effect(s) tested	The effect of preprocessing pipeline on neighboring DWI correlation (NDC) and smoothness (full-width at half maximum, FWHM).
Specify type of analysis:	<input checked="" type="checkbox"/> Whole brain <input type="checkbox"/> ROI-based <input type="checkbox"/> Both
Statistic type for inference (See <a href="#">Eklund et al. 2016</a> )	Whole-brain summary measures
Correction	Bonferroni correction was applied across statistical tests

## Models & analysis

n/a	Involvement in the study
<input checked="" type="checkbox"/>	<input type="checkbox"/> Functional and/or effective connectivity
<input checked="" type="checkbox"/>	<input type="checkbox"/> Graph analysis
<input checked="" type="checkbox"/>	<input type="checkbox"/> Multivariate modeling or predictive analysis